Arab J Geosci (2012) 5:1163–1172
DOI 10.1007/s12517-010-0255-6

COMMENT

Detection of subsurface faults with seismic and magnetic methods

Sherif M. Hanafy · Essam Aboud · H. S. A. Mesbah

Received: 10 June 2010 / Accepted: 29 November 2010 / Published online: 22 December 2010

Abstract In this work, we used seismic refraction and magnetic methods to find the extension of a known subsurface fault and delineate for the existence of many others. Combination of both seismic refraction and magnetic method give a better subsurface view, where both seismic and magnetic methods can detect fault locations; however, fault thrown and subsurface layering will be better detected by seismic method, while magnetic method will provide a better lateral view of the faulting system in the study area. Seismic refraction shows that at least two fault plans exist in the subsurface; magnetic results supported seismic results and suggested the existence of several small fault plans in the study area.

Keywords Seismic refraction · Magnetic · Subsurface fault · Fault system · Fault plan

Introduction

Over the last 20 years, 6th October City in Egypt was seen to have heavy development in urbanization and industrial activity. It is planned that such developments will expand in the future. In that regard, soil engineering characteristics constitute one of the cornerstones for any new urbanization expansion.

S. M. Hanafy
Department of Geophysics, Faculty of Science, Cairo University, Cairo, Egypt

E. Aboud · H. S. A. Mesbah (✉)
National Research Institute of Astronomy and Geophysics, Helwan,
Cairo, Egypt
e-mail: hmesbah2000@yahoo.com

Seismic refraction and magnetic methods are used to investigate the subsurface layering and structure. These techniques are routinely used in many applications, such as engineering, environmental, groundwater, hydrocarbon, and mineral exploration (Khalil and Hanafy Sh 2008; Khalil et al. 2008; Bridle 2006; Yilmaz et al. 2006; Hodgkinson and Brown 2005). In this work, we used both techniques to get a better view of the subsurface layering and structure elements. The integrated results from both techniques give more accurate view of the subsurface in both lateral and vertical direction.

The traditional interpretation of seismic refraction data has used a concept of layered horizons, where each layer has a discrete seismic velocity. New interpretation techniques analyze and present seismic velocity as a continuously varying gradient across a grid or mesh. Such techniques may utilize optimizing methods coupled with finite element or finite difference concepts to achieve interpretations. These techniques have advantages and disadvantages with respect to the traditional seismic refraction interpretation techniques. Advantages of the former techniques include better velocity-depth models, while disadvantages include requirement of bigger quantity of collected data and processing time. In the present study, due to the limited number of collected data, traditional seismic technique is used, where seismic data are conducted and interpreted, using a combination of Plus–minus (Hagedoorn 1958) method and reciprocal (Hawkins 1961) method, and then a finite difference technique is applied to test the accuracy of the final velocity-depth model.

Modern high-resolution magnetic surveys are able to detect magnetic signatures in the subsurface and trace the extension of the faults. The main issue in the magnetic method is the ambiguity in the interpretation, which could have various possibilities for the interpretations. In this

regard, we used the gradient interpretation methods that use the derivatives (gradients) of the field in their calculation, such as Euler deconvolution, tilt derivative. Using Fast Fourier Transform (FFT) in calculating the derivatives (two horizontal and one vertical) of the field make these methods more advanced. Early in 1970s, a variety of automatic and semiautomatic methods, based on the use of gradients of the potential field, have been developed as efficient tools for determination of parameters, such as locations of boundaries and depth of the causative sources (Aboud 2005)

The success of these methods results from the fact that quantitative or semiquantitative solutions are found with no

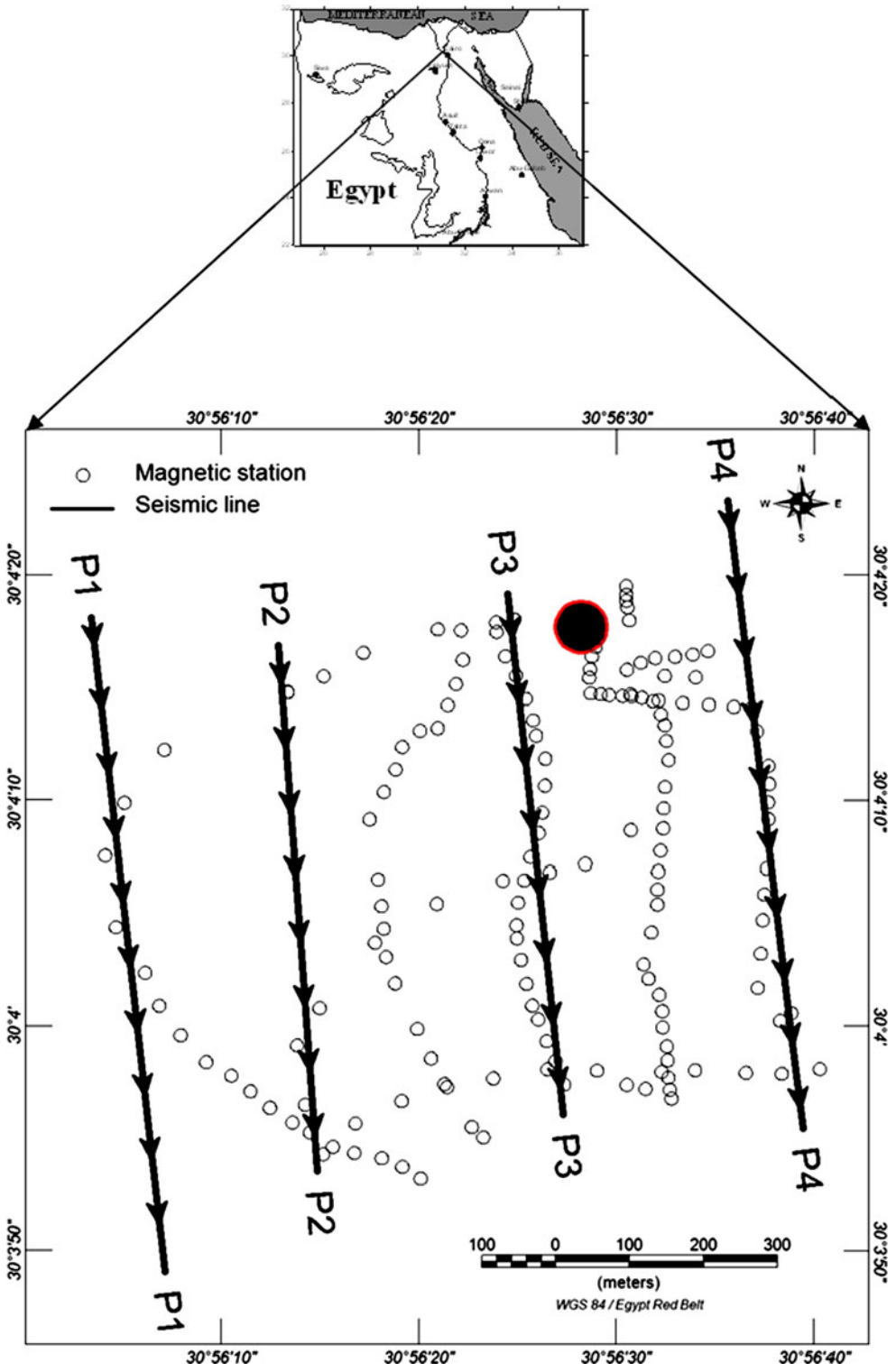

Fig. 1 The location of magnetic survey and seismic lines at the study area. The *arrows* show the direction of seismic lines and the *black-filled circle* shows the location of magnetic base station

or few assumptions. For instance, Euler deconvolution, which is used to estimate the location and depth of magnetic source, can be applied to the magnetic data without any priori geologic information (Reid et al. 1990 and Thompson 1982). Recently, combination of these method facilitates can accelerate the interpretation of the data. In our study, the two gradient methods (Euler deconvolution and analytic signal) will be used simultaneously in order to well understand the subsurface structures.

Geological background

The area of study is located east of Qaret El Haddadin, 6th October City, which is 15 km north of Cairo, Egypt (Fig. 1). The area is mainly covered with two types of rocks, they are:

1- El Haddadin Basalt (Fig. 2), which is Oligo-Miocene age, can be subdivided into three layers from bottom to top (Shallaly 1992):

a. Lower amygdaloidal basalt
b. Strongly porphyritic basalt
c. Upper amygdaloidal basalt

The lower amygdaloidal basaltic flow appears mostly in Gabal Qattrani, but in the study area, it is mainly absent due to fault action. The strongly porphyritic basaltic flow is plagioclase, pyroxene, massive, and fresh. It exhibits vesicular top, which is scarcely seen, owing to erosion and fault action. The upper amygdaloidal basaltic flow is composed of ten superimposed, flat-laying terrace-forming sheet. It is supremely altered.

Most of the trenches found in the study area (wastewater pipe trenches) bare the upper most 3.5 m of the strongly porphyritic basalt, which is hard, greenish black. The overlaying upper amygdaloidal basalt is about 1.5-m thick; it is of purple color, and features large, irregular vesicles and filled with green earths. The contact between the previously mentioned layers is sharp.

The upper amygdaloidal basalt layer (which can be considered the foundation layer) occurs in the form of a compound lava flow that is made up of ten terrace-like successive sheets without professed weathering surfaces in between. The thickness of this flow is about 15 m; color varies from brownish black on the bottom to black on the top, passing with the purplish and grayish colors in the middle.

2. Gabal El Khashab Formation (Lower Miocene). Overlaying the upper amygdaloidal basalt layer is a series of alluvial

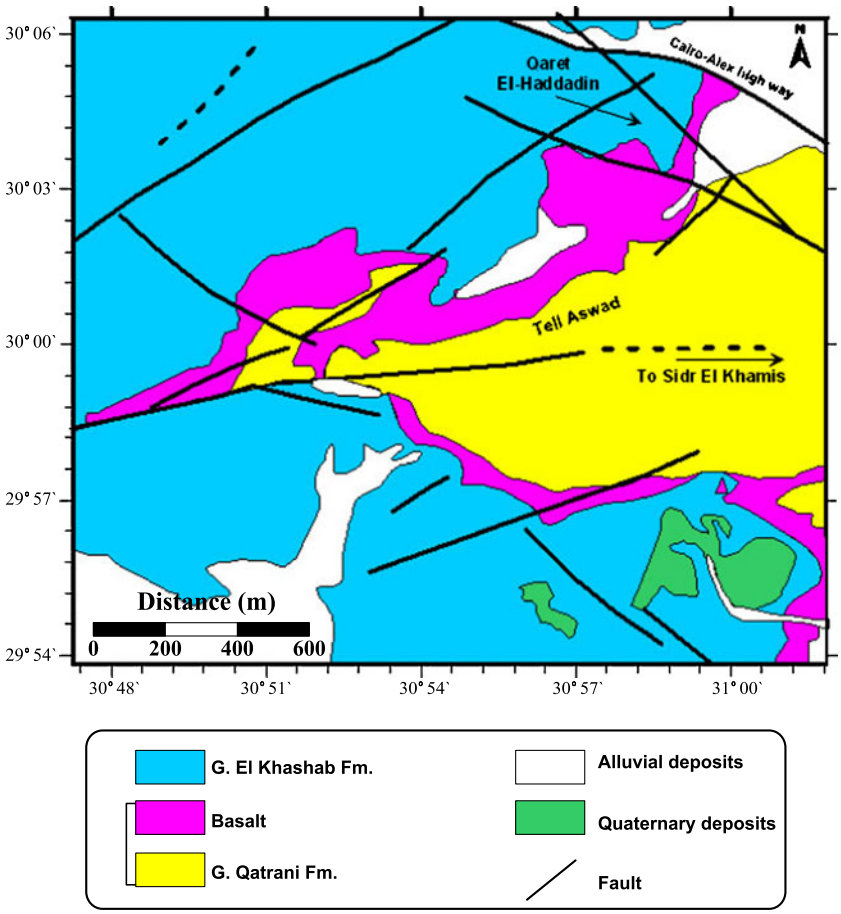

Fig. 2 Geological map of the study area (*star*) and its surroundings

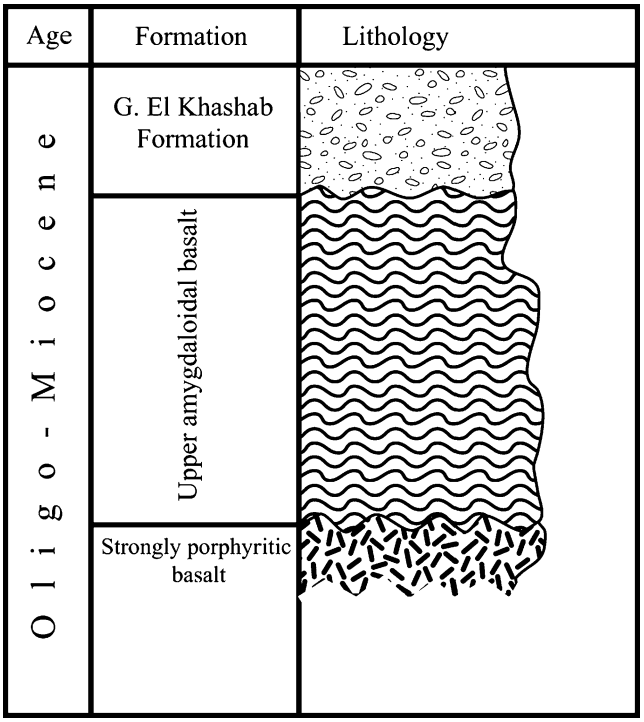

Fig. 3 Stratigraphic section of the study area

sands and gravels, which is known as Gabal El Khashab red beds (Figs. 2 and 3). The formation derived its name from the innumerable silicified logs that occur in it and strewn across broad areas of the desert north of the Fayum Depression.

The formation mainly consists of gravelly sandstones, red and orange, medium to coarse-grained sandstones, which are plane-bedded and large scales cross-through-stratified with red and drab mudstones. (Bown and Mary 1988). Freshwater shells and numerous marine *Scutella* remains are jotted down from these beds (Said 1962).

The contact between the Gabal El Khashab Formation and the underlying basalt layer is markedly erosional, and scours in the top of the basalt are filled with coarse sand, sometimes containing basalt debris and chert-pebble conglomerate. Weathering of the rather common chert-pebble and cobble conglomerates has produced a desert pavement.

Seismic refraction acquisition and interpretation

A total of four profiles were collected at the study area (Fig. 1). We used the ES-3000 seismograph for data acquisition. It has 12 channels. Here, we used 5 and 7.5 m as geophone intervals and a sledge hammer 8 kgm as seismic sources. Seismic vibrations traveled inside the rock layers; they are partially reflected and partially refracted at layer boundaries. The refracted portion of the seismic waves is returned to the ground surface and recorded at the geophone points.

The collected data are interpreted using SeismicImager Software Version 3.14. The collected data are first plotted (Fig. 4) and filtered using a band-pass filter. The first

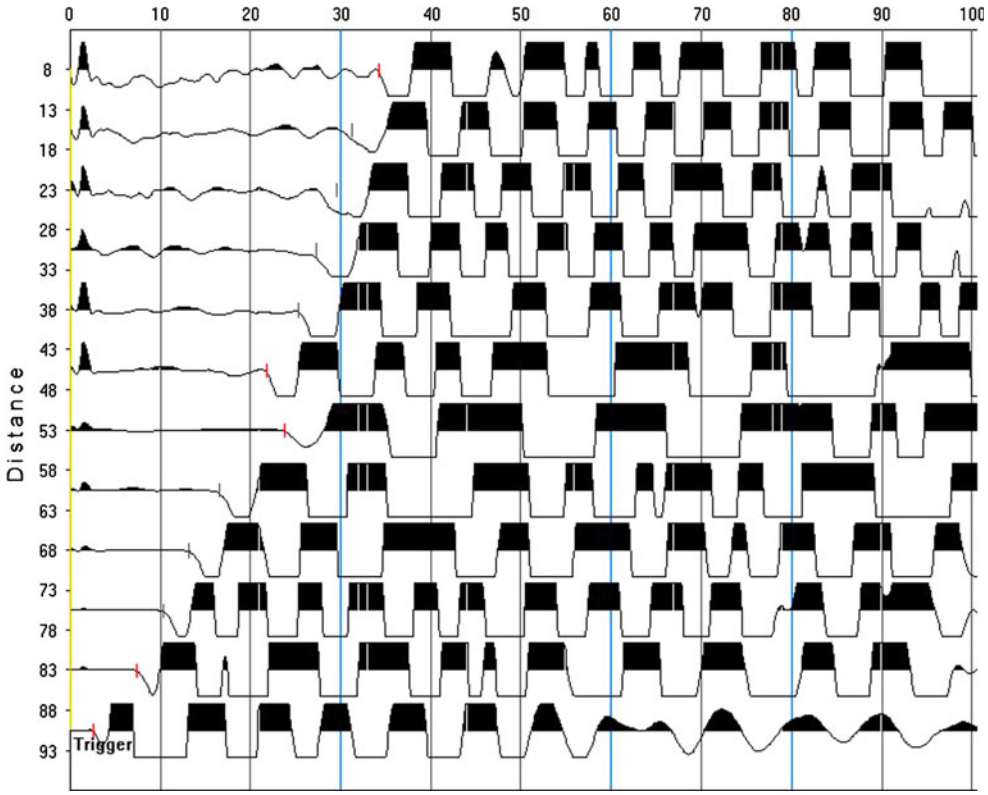

Fig. 4 Seismogram sample after band-pass filter. *Vertical red lines* show the picked first-arrival times

arrivals are then picked (Figs. 4 and 5). All picked first-arrival travel times (Fig. 5) are introduced to the interpretation software and each profile is separately interpreted to generate the corresponding velocity-depth (V-D) section. Both reciprocal (Hawkins 1961) method and plus–minus (Hagedoorn 1958) method are used to interpret the seismic refraction data, and the outputs (V-D sections) are then gently smoothed and verified with finite-difference method (Hanafy 2005). Results are shown in Fig. 6 and listed in Table 1.

Four layers can be shown in the study area; they are from top to bottom:

1. A surface layer corresponding to lose sand sediments.
2. Second layer corresponds to sandstone or compacted sand layer.

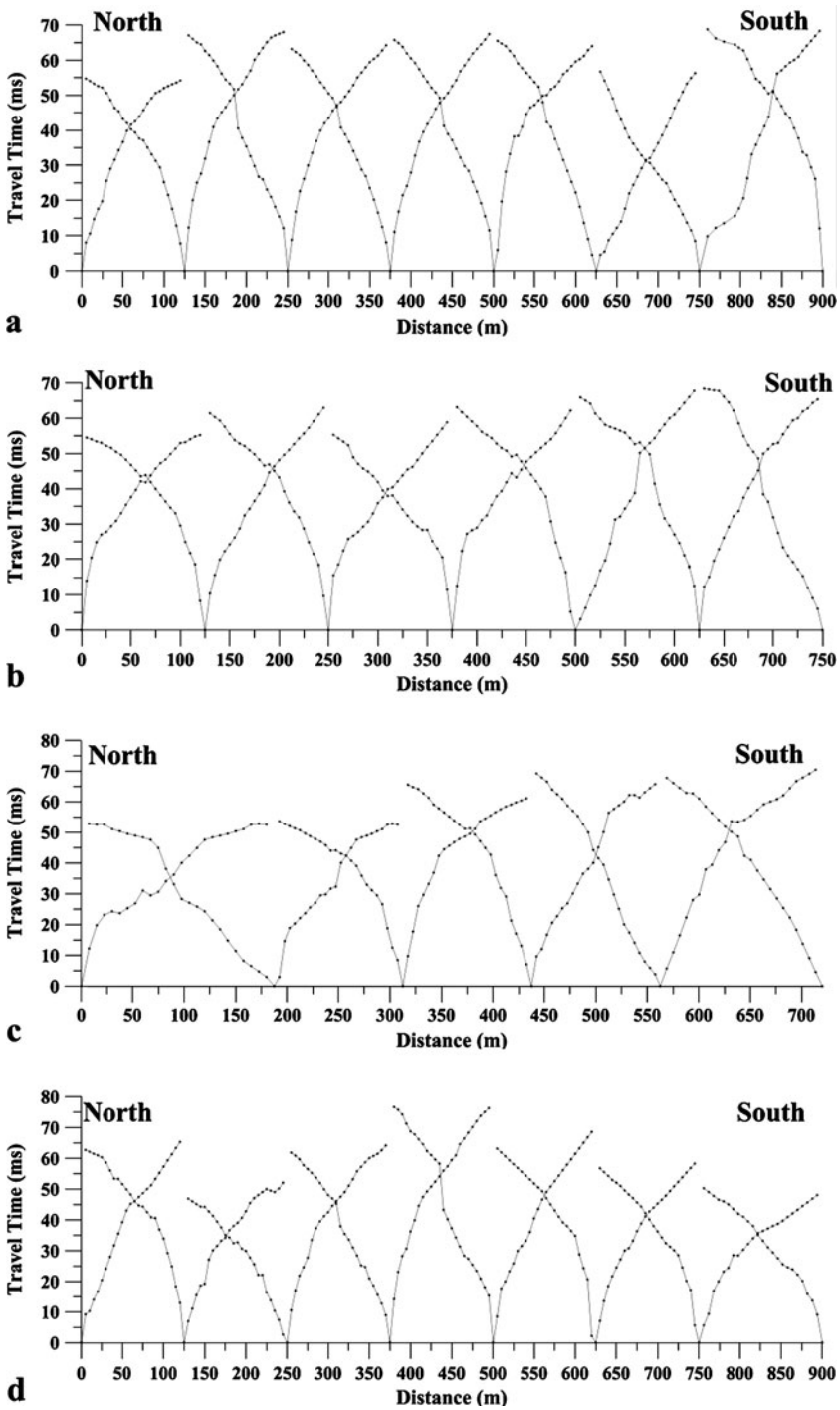

Fig. 5 First-arrival travel times of the collected four seismic profiles. **a** to **d** are profiles 1 to 4, respectively

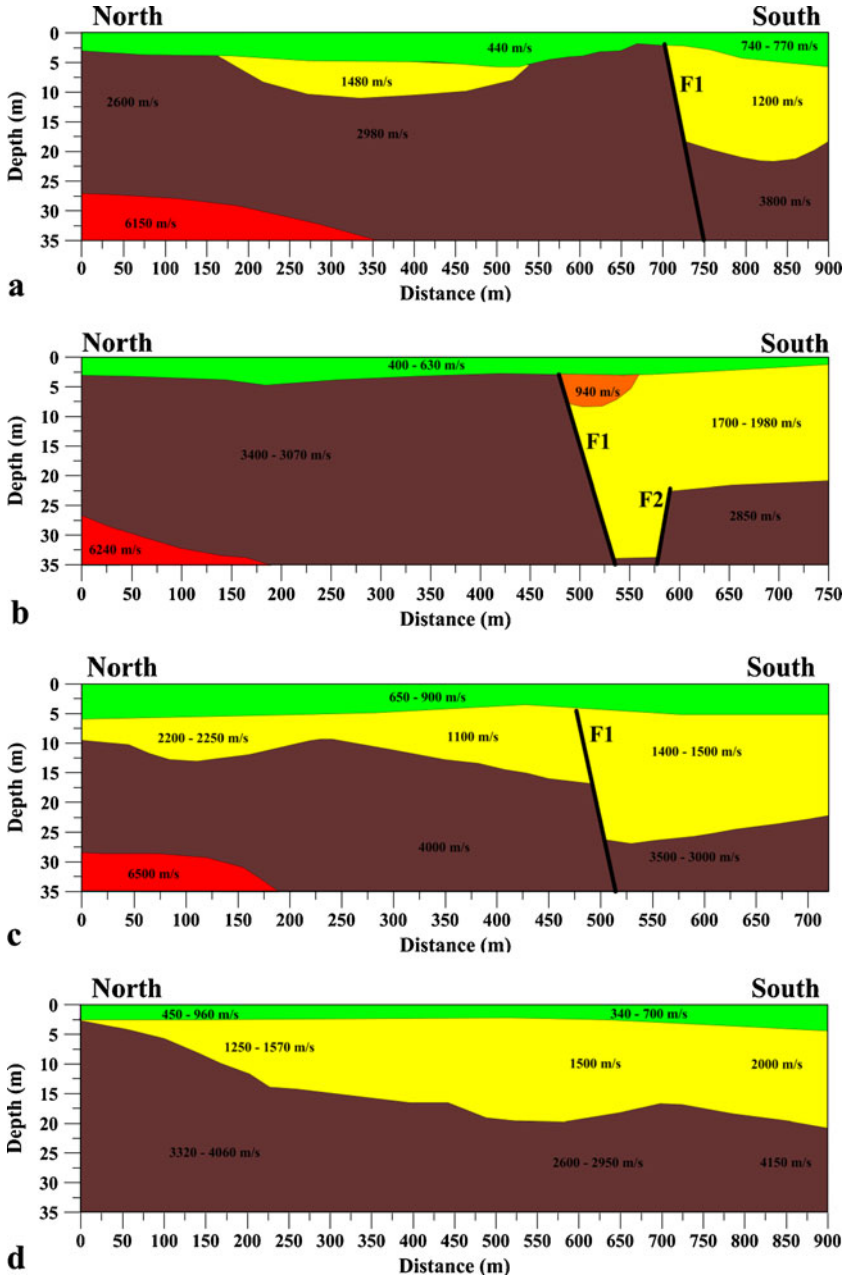

Fig. 6 Velocity-depth sections of the collected four seismic profiles. **a** to **d** are profiles 1 to 4, respectively

Table 1 Summary of the seismic refraction interpretation shows the layer thickness, velocity ranges, and lithology

Profile	Length	Layer 1			Layer 2			Layer 3			Layer 4		
		h (m)	V (m/s)	L	h (m)	V (m/s)	L	h (m)	V (m/s)	L	h (m)	V (m/s)	L
1	900	2–5	440–770	I	0–20	1,200–1,480	I	-|-	2,600–3,800	I	-|-	6,150	I
2	750	2–4	400–630	II	15–25	1,700–1,980	II	-|-	2,850–3,400	II	-|-	6,240	II
3	750	4–6	650–900	III	5–20	1,100–2,250	III	-|-	3,000–4,000	III	-|-	6,500	III
4	900	2–4	340–960	IV	0–12	1,250–2,000	IV	-|-	2,600–4,120	IV	–	–	IV

h, thickness; *L*, lithology (from bore holes); *V*, velocity; -|-, extend to the bottom of section; –, layer does not exist; *I*, loose sand; *II*, sandstone layer (or compacted sand); *III*, altered basalt; *IV*, basal

3. Third layer corresponds to altered (weathered) basalt; the higher the velocity the lower the weathering effect.
4. Fourth layer corresponds to fresh basalt and is shown only at the northern part of each section except in section 1, where it is missing (could appear at greater depths).

Two faults are shown on the sections (F1 and F2), both of them are normal faults. The faults are the main reasons that make the second layer disappear in some parts of the study area. Fault (F1) is running east–west with upthrown at the northern part of the study area and downthrown at the southern part. Fault (F1) appears in seismic profile #s 1, 2, and 3 and does not appear in seismic profile #4, while fault (F2) appears only on seismic profile #2, which suggests that F2 is either a small fault segment, or it runs in a different direction and is not detected by seismic profiles. Fault (F2) shows that the upthrown is at the southern part of the study area and downthrown is at the northern part. Magnetic study will give a better view of the faulting system in the area of the study, their locations, and orientation.

In seismic profile #4, the thickness of the second layer changes from 0 m at the north to more than 20 m at the south (Fig. 6d). There are two possible interpretations here. First, there is a subsurface normal fault between offsets X= 150 and X=200 m. Second, the thickness of the second layer is increasing gradually from north to south. We choose the latter interpretation, since there is no geological or magnetic (see latter) evidence of any subsurface faults in this part of the study area.

Magnetic data acquisition and interpretation

The study area is covered with magnetic survey, using the GSM-19 Overhauser magnetometer in order to detect the subsurface structure. The used system is designed to measure the total field and/or gradient field, and is essentially proton precession devices.

A base station with magnetic homogeneity was selected within the study area as shown in Fig. (1) to correct the data for the diurnal variation. Due to the small size of the study area (1 km^2), the station interval was about 25–50 m. Figure 1 shows the locations of the magnetic measurements (black circles) that covers the study area.

The magnetic survey covered most of the area, except some locations due steel fancies in the area. Base station data was used to correct the rollover data, and finally, a total intensity magnetic anomaly map was produced, reflecting the subsurface structure (Fig. 7).

The total intensity magnetic anomaly map of Beverly Hills area (Fig. 7) shows high magnetic anomalies over the eastern, western, and northern parts of the area, which indicate the presence of magnetic rocks covering these parts, since the geological surface does not reflect the

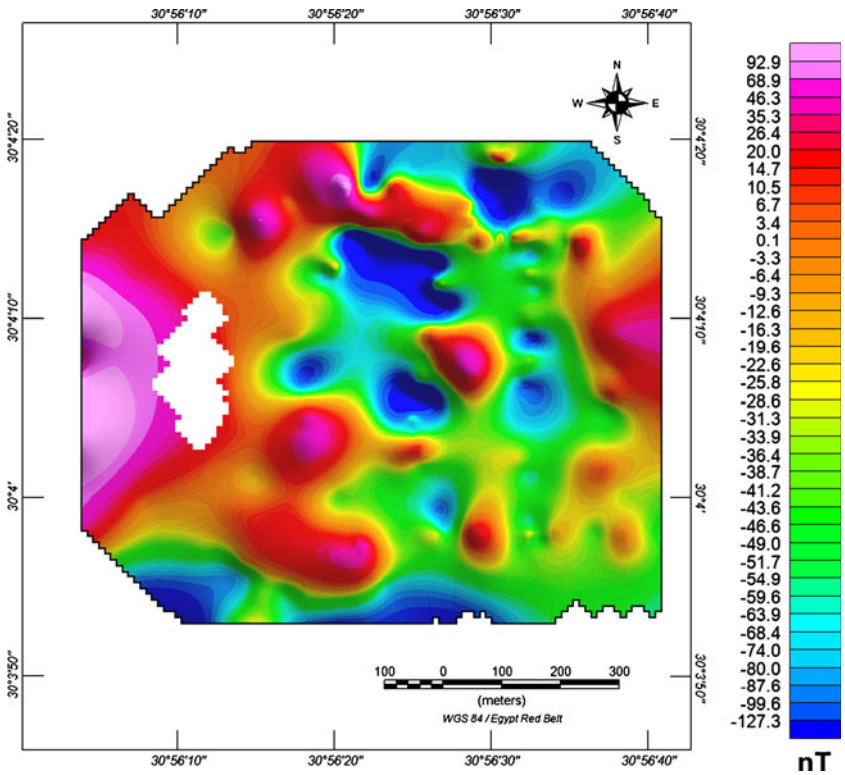

Fig. 7 The total intensity magnetic anomaly map of Beverly Hills area, Egypt. The *white area* indicates the lack of the data due to inaccessibility (steel fancies)

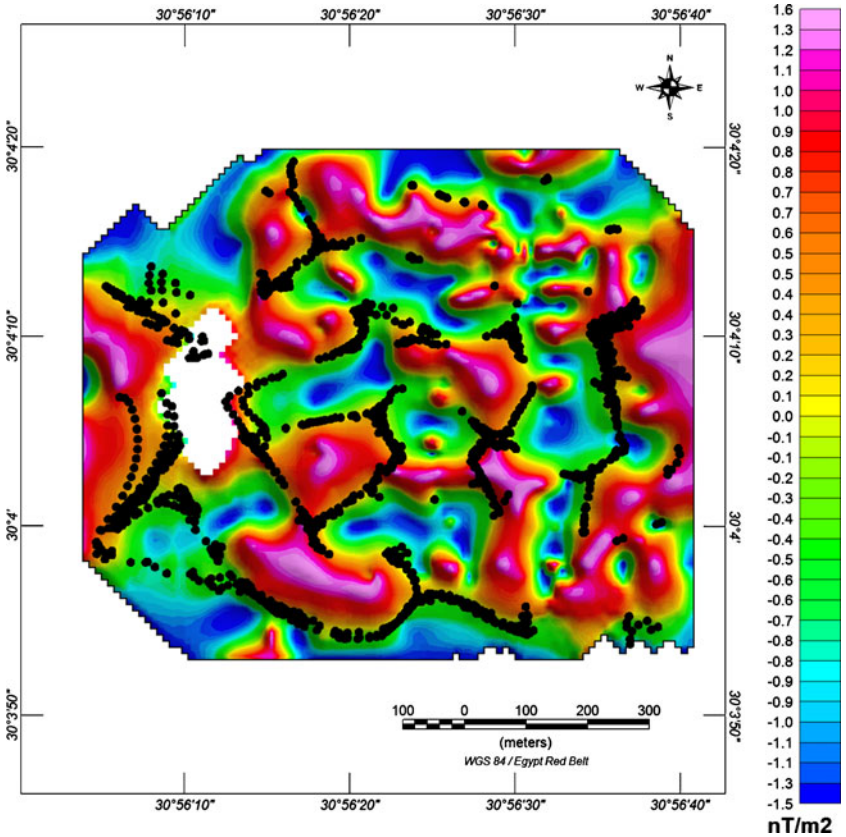

Fig. 8 The output results from TDR (*zero contour line*) and Euler method (*black filled circles*). The background image is the TDR grid

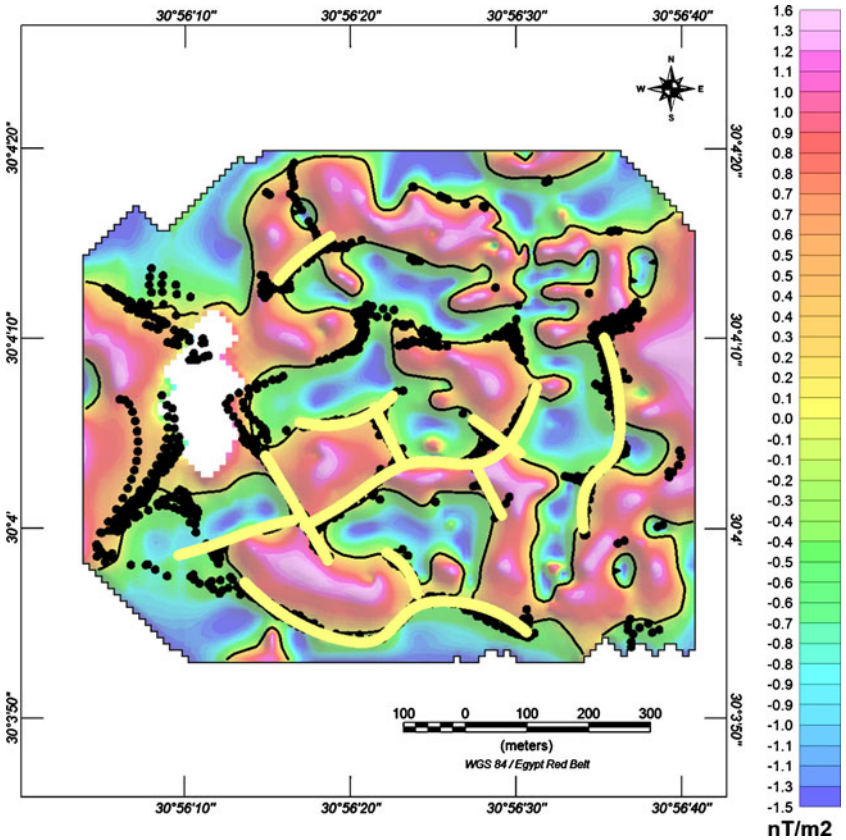

Fig. 9 *Yellow solid lines* representing the fault plans, where both TDR and Euler methods agree. *Red dashed lines* represent the two faults from seismic interpretation

presence of any magnetic rocks. Hence, these high magnetic values could be due to the presence of basaltic rocks beneath the surface.

Magnetic data alone gives a general idea about the subsurface structures affecting the study area. Processing the magnetic data enhances and sharpens the anomalies and trends of the data and helps in the interpretation. In this work, we will apply two techniques in order to estimate the locations of the subsurface faults.

First, we will utilize the Tilt Derivative filter (TDR) that is usually used to detect the geological edges/contacts. The TDR and its total horizontal derivative are useful for mapping shallow basement structures and mineral exploration targets. This filter is estimated by dividing the vertical derivative by the total horizontal derivative Verduzco (2004) as below.

$$\mathrm{TDR} = \arctan\left(\mathrm{VDR}/\mathrm{THDR}\right) \tag{1}$$

where VDR and THDR are the first vertical and total horizontal derivatives, respectively, of the total magnetic intensity *T*.

$$\mathrm{VDR} = \mathrm{d}T/\mathrm{d}z \tag{2}$$

$$\mathrm{THDR} = \mathrm{sqrt}\left((\mathrm{d}T/\mathrm{d}x)^2 + (\mathrm{d}T/\mathrm{d}y)^2\right) \tag{3}$$

The most advantage of the TDR is that its zero contour line is on or close to the fault/contact location.

Second, we will apply Euler deconvolution method (Reid et al. 1990) to estimate the depths to the contacts that delineated, using TDR. In this study, we applied magnetic measurements to delineate fault system in the study area. Theoretically, 0 is the appropriate structural index for contact, as would apply to fault. However, this structural index usually gives unstable results (Barbosa et al. 1999). Reid et al. (1990) showed that the lower structural indices (SIs) ranging from 0 to 1 are better contact locator. In our study, several SIs were selected (from 0 to 0.5). Then, by inspecting the results, the optimal structural index that yielded the best clustering of solutions was chosen. Based on these trails, 0.5 is selected as SI and applied to the magnetic data of the study area.

Figure 8 shows the output results from the TDR and Euler deconvolution method. The TDR results are represented by its zero contour line (black lines), while Euler results are represented by black-filled circles showing the locations of the faults. It could be recognized that both the two methods showed coherent results, which increase the certainty in our solution. However, in some locations, the results are not matched, which could be interpreted due to the limitations of the methods.

In order to locate the contacts/faults, the locations at which TDR and Euler methods are matched, will be traced and interpreted as faults. Figure 9 shows the traced faults from magnetic data (yellow solid lines). It is clear that the main trend of the area is in the EW direction and some other trends are in NS, and NE–SW.

Conclusions

In this paper, we used two geophysical techniques (seismic refraction and magnetic) to investigate the area of study. These methods are used to delineate the subsurface sediments and the structure elements in the area of study. A total of four seismic refraction profiles and 156 magnetic stations were conducted. Interpretation of the seismic refraction profiles shows the existence of four subsurface layers and two normal faults. The subsurface layers are (1) a surface layer corresponding to loose sand sediments; (2) next layer corresponds to sandstone or compacted sand layer; (3) third layer corresponds to altered (weathered) basalt; and (4) last layer corresponds to fresh basalt. Fault (F1) is running east–west with upthrown at the northern part of the study area and downthrown at the southern part, while fault (F2) has upthrown at the southern part of the study area and its downthrown is at the northern part. Fault (F1) appears in all four seismic profiles and fault (F2) appears only on seismic profile #2.

Magnetic readings are interpreted using two methods; TDR and Euler methods. Both methods can determine the lateral location of fault plans. In order to locate the faults in the study area, the locations at which TDR and Euler methods are matched, will be traced and interpreted as faults contact.

Comparing locations of fault plans from both seismic and magnetic methods show that they agree. Magnetic method is able to detect the fault planes (F1 and F2) that are detected by seismic method. Advantage of magnetic method is that more fault planes are detected, while advantage of seismic method is that fault depths and thrown can be easily determined, as well as the thickness of the subsurface sediments in the study area.

References

Aboud E (2005) Development in magnetic data interpretation technique using Euler deconvolution and analytic signal methods, PhD thesis. Kyushu Univ, Japan

Barbosa VCF, Silva JBC, Mederios WE (1999) Stability analysis and improvement of structure index estimation in Euler deconvolution. Geophysics 64:48–60

Bown MT, Mary KJ (1988) Geology and paleoenvironment of the Oligocene Jebel Qatrani Formation and adjacent rocks, Fayum Depression, Egypt. Geol Surv Prof Pap 1452:60

Bridle R (2006) Plus/Minus refraction method applied to 3D block. SEG Expanded Abstracts 25, 1421. from magnetic data:. Geophysics 47:31–37

Hagedoorn JG (1958) The plus-minus method of interpreting seismic refraction sections. 15th meeting of European Association of Exploration Geophysicists, London

Hanafy ShM (2005) Seismic refraction interpretation using finite difference method. SAGEEP 2005:1012–1024

Hawkins LV (1961) The reciprocal method of routine shallow seismic refraction investigations. Geophysics 26(6):806–819

Hodgkinson J, Brown RJ (2005) Refraction across an angular unconformity between nonparallel TI media. Geophysics 70:D19

Khalil MH, Hanafy Sh M (2008) Engineering applications of geophysics: A field example at Wadi Wardan, northeast Gulf of Suez, Sinai, Egypt. J appl geophys 65:132–141

Khalil MH, Hanafy ShM, Gamal MA (2008) Preliminary seismic hazard assessment, shallow seismic refraction and resistivity sounding studies for future urban planning at the Gebel Umm Baraqa area, Egypt. J Of Geophysical Engineering 5:371–386

Reid AB, Allsop JM, Granser H, Millett AJ, Somerton IW (1990) Magnetic interpretation in three dimensions using Euler Deconvolution. Geophysics 55:80–90

Said, R., 1962, The Geology of Egypt, El Sevier Publishing Company, p. 104

Shallaly N (1992) Geology and tectonic setting of the basalts and associated rocks, El Fayum area. M.SC. Cairo University, Western Desert, Egypt

Thompson DT (1982) EULDPH: A new technique for making computer-assisted depth. Geophysics 47:31. doi:10.1190/1.1441278

Verduzco B (2004) New insights into magnetic derivatives for structural mapping. Leading Edge, The 23:116–119

Yilmaz O, Eser M, Berilgen M (2006) Seismic, geotechnical, and earthquake engineering site characterization. SEG Expanded Abstracts 25:1401